Journal of Applied Mechanics Vol.10, pp.351-362 (August 2007) JSCE

Laboratory Model Test and Numerical Analysis of Bearing Capacity of Rigid Strip Footing

Liang LU*, Katsuhiko ARAI**, Zongjian WANG*

*Nonmember, Doctoral Programs, Graduate Schoole of Eng., University of Fukui (Bunkyo 3-9-1, Fukui 910-8507)
**Fellow, Dr. Eng., Prof., Dept. of Architecture and Civil Eng., University of Fukui

This paper reports the results of laboratory model tests subjected to bearing capacity of rigid strip footing. Based on the results, this paper proposes a numerical procedure for estimating the bearing capacity of rigid strip footing under some complex conditions. The procedure uses a smeared shear band approach and a modified initial stress method to provide an explicit collapse mechanism represented by the stress yield condition, assuming the Mohr-Coulomb yield criterion with a simple non-associated flow rule. The procedure employs a simple constitutive model which requires a small number of soil parameters, so that it may be applied to practical design work rather than the simulation of actual failure behavior. Comparison is made between the results calculated by the numerical procedures and those of the laboratory model tests.

Key Words: *bearing capacity, laboratory model test, slip surface, shear band, initial stress method*

1. Introduction

Conventional stability analysis based on the limit equilibrium method and so on, is as yet the most powerful means for estimating the bearing capacity of rigid strip footing. However the stability analysis often tends to become uncertain and unreliable for a soil stratum which consists of multiple layers, or which includes materials having quite different stiffness. This is because the stability analysis does not consider the stiffness of materials, but evaluates the material properties only by its final strength. At first, laboratory model tests are carried out to evaluate the actual behavior of settlement and collapse mode of soil stratum under footing pressure. Secondly, based on the findings of the model test, proposed is a numerical procedure for bearing capacity, which considers the stiffness and strength of materials. Based on a smeared shear band approach and a modified initial stress method, assuming Mohr-Coulomb yield criterion with a simple non-associated flow rule, the proposed procedure attempts to provide an appropriate bearing capacity which is supported by an explicit collapse mechanism represented by stress yield condition. This method employs a simple constitutive model which requires a small number of material parameters, so that it may be applied design work rather than the simulation of actual failure behavior.

2. Laboratory Model Test

2.1 Test Equipment

Fig. 1 shows the soil container made of steel, which is used for laboratory model test. The inner size of the soil container is shown in Fig.1. In order to observe the experimental behavior, a hardened glass with grids of 5cm size is fixed on one side of the soil stratum. Earth pressure meters are installed in the ground (as shown in Fig. 2) to measure vertical earth pressure. A laser telemeter is used to measure the settlement of loading plate. Beans or colorful sands are interspersed in layers among the soils which enable to visualize the formation of active failure wedge under footing. Considering the friction between soil stratum and soil container, we use a thin rubber membrane smeared with a thin layer of silicon grease on the surface of side walls of soil container. We perform also the other model test without rubber membrane, and compare the friction effect to bearing capacity. To apply loads to the loading plate, a Bellofram Cylinder is used, in which the air pressure obtained from air compressor. We use two sizes of loading plate, 10cm and 15cm in width. A sand paper is glued onto the undersurface of loading plate, so that it may simulate rough condition on base friction.

2.2 Soil Material

Considering the specimen characteristics and size effect of

loading plate, the model tests are performed based on three different types of subsoil made of dense (Toyoura) sand, loose (Toyoura) sand and mountain sand respectively. Table 1 lists the soil parameters, where E: Young's modulus of the soil stratum, B: width of loading plate, μ: Poisson's ratio, and c, ϕ: Mohr-Coulomb strength parameters. c and ϕ are obtained by a direct shear test. E is back-calculated by the footing settlement observed. The elastic modulus of geotextile is determined by a tensile test. Y denotes the model test with geotextile, while N denotes the test without geotextile. Material properties of geotextile (polyester) are as follows, length: 900mm, width: 200mm, thickness: 0.21mm, tensile strength: 117.6kN/m^2, strain at tensile failure: 19%, mass density: 130g/m^2, E: 1200MN/m^2. A piece of geotextile is put on the location shown in Fig.25.

2.3 Test Procedure

As stated above, foundation subsoil is made respectively of three types of soil material shown in Table 1, which is assumed to be homogenous. For normal sand, the subsoil is produced by spreading equipment, which is a vessel of triangular prism with a spindly vessel. The spreading equipment is suspended on a hoist, and travels at a constant speed, by which the sands dropped into the soil container uniformly through a screen with 16 meshes. The vessel can be used to adjust the density of filling by altering the magnitude of nozzle. The nozzle size of 2mm is used for dense sand, while 10mm for loose sand. For mountain sand, the foundation subsoil is manufactured by step loading. Firstly, after the filling is added to the position on which earth pressure meters installed, the load of 24.78kg in weight are pressed on the soil layer for 2 minutes to compress subsoil. Secondly, earth pressure meters and colorful beans are placed, and afterwards sands are added to the scheduled height of soil container. Finally, the subsoil is compressed by the way of four phases' loads of 24.5kPa, 49kPa, 73.5kPa and 98kPa. In the early three phases the pressure is kept for 2 minutes and the last phase for 5 minutes.

After completing the subsoil, a loading plate is put on the subsoil, on which loading pressure is applied by Bellofram Cylinder. The subsequent process is summarized as: (1) An increment of load to the loading plate is applied and kept constant. The amount of increment was decided by considering the bearing capacity, so that the steps of loading may become about 10 to 20. (2) After three minutes, the settlement of loading plate and the earth pressure corresponding to current load are measured. (3) Repeat steps 1 and 2 until the failure of subsoil.

2.4 Test Results

Test results show that the bearing capacity is considerably affected by many test conditions, such as friction of sidewall of container, placement of earth pressure meters, and so on. The case when we set lubricating membrane on the sidewall is called frictionless case, and the case when we use no membrane is friction case. Fig. 3 shows that the bearing

Table 1. Properties and conditions of soil specimen

Soil type	dense sand		loose sand		mountain sand	
loading plate width: B (cm)	10	15	10	15	10	15
c (kPa)	0		0		12.25	
ϕ	41.38°		29.78°		30.96°	
E (kPa)	3924		981		3924	
γ (kN/m^3)	15.928		14.034		15.66	
D_{50}(mm)	0.12		0.12		0.35	
μ	0.33					
geotextile	N	Y	N	Y	N	Y

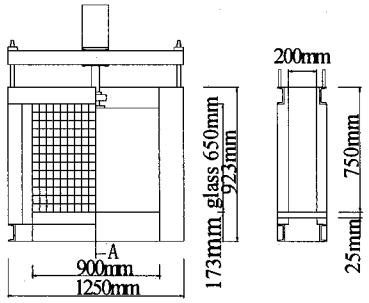

Fig. 1 Soil container

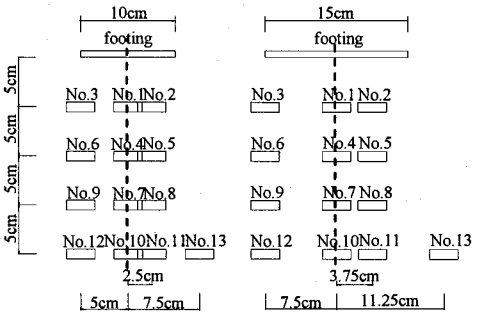

Fig. 2 Distribution of earth pressure meters

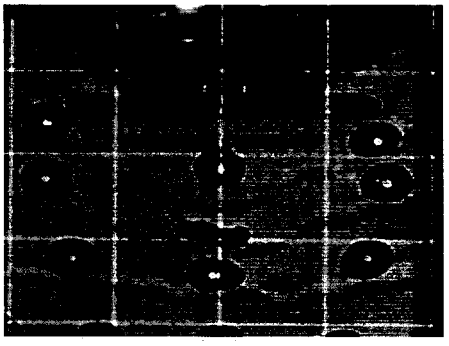

Photo. 1 Formation of active wedge (dense sand, B=15cm)

capacity in frictionless case is smaller than that of friction case for dense sand, while there is not so much difference for loose sand. Fig. 4 shows that the placement of earth pressure meters may improve bearing capacity, due to the reinforcement effect. Fig. 5 compares the results performed on the same condition for investigating scatter in test result. For dense sand, due to time lag of construction of global collapse mode, test result scatters remarkably, while for loose sand the probability of reappearance is high. Hereafter we employ only the test result under the condition of frictionless case and placing earth pressure meters. Fig. 6 shows the effect of earth reinforcement. In dense sand case, we can obtain the clear failure point. In Fig. 6 (a), in any condition an active wedge below footing has been formed (see Photo. 1) and explicit slip surface is observed before the settlement increases remarkably. In Figs. 6 (b) and 6 (c), the evident active wedge cannot be observed. In any case the earth reinforcement gives much larger bearing capacity. Fig. 7 illustrates only a part of vertical earth pressures monitored. The earth pressure near the centerline tends to increase after failure, while the pressure apart from center decreases. This phenomenon may be related to the occurrence of active wedge under footing.

3. Numerical Procedures 1

3.1 Outline

Many analytical and numerical techniques can be used to calculate the bearing capacity of a rigid strip footing. The conventional stability analysis is based on the limit equilibrium method, slip line method and so on. The limit equilibrium method represents kinematical conditions only by using the mechanically reasonable shape of a slip surface as shown later in Fig. 12, and evaluates the material properties only by its final strength. The method does not explicitly allow to consider the stiffness and deformation of materials which may play an important role for evaluating earth reinforcement, and which may affect the globe collapse mode. Due to the defect, some methods are proposed. Many researches indicate that classical FEM does not necessarily provide a reasonable collapse mechanism[1),2)]. Subjected to Mohr-Coulomb material, the limit analysis has not completely overcome the difficulty that the limit theorems cannot be proven without the normality rule in plasticity, and that the normality rule may not hold for the material, although it is known that the analysis provides a suitable solution in most cases[3)-5)]. In spite of many researches, the accurate description of localization phenomenon in soils is still open to question. For instance, the bifurcation analysis that tries to simulate actual localized deformation seems to give a promising view, while the analysis may not give reasonable solutions for complicated boundary value problems like

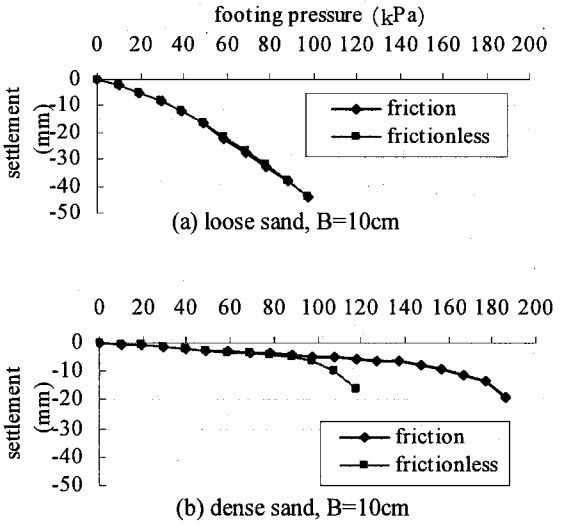

Fig. 3 Effect of sidewall friction

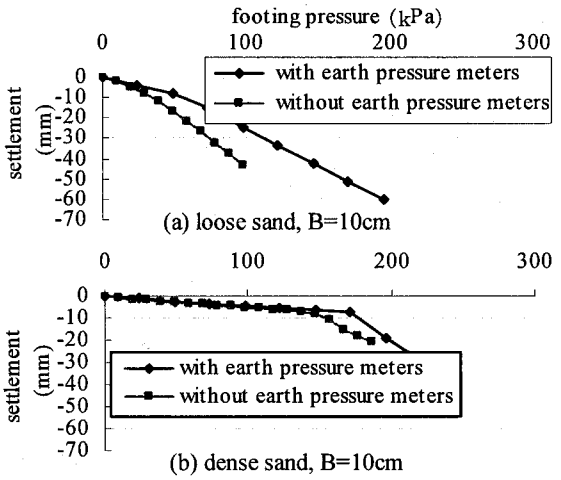

Fig. 4 Effect of placing earth pressure meters (frictionless)

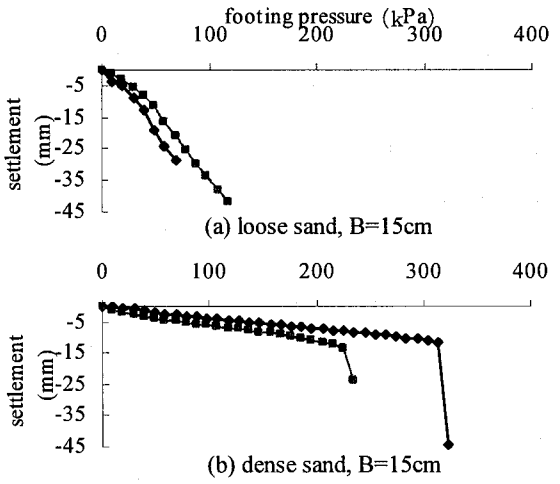

Fig. 5 Dispersion of test results (frictionless)

bearing capacity[6),7)]. This may be because in bearing capacity problems it is not easy to duplicate the rotation of principal stresses from the below part of footing to the peripheral region.

The adaptive procedure appears to require a lot of numerical efforts and to contain a certain numerical difficulty in some cases[8), 9)]. In this paper, based on a modification of smeared shear band approach[10)] and on a new calculation scheme for nonlinear FE analysis, a simple and practical procedure for estimating the bearing capacity is discussed, which enables to create a reasonable collapse mode. The conditions to get such a collapse mode are as follows: 1) Assume an active wedge below footing, 2) Treat the yielding mass as a stratified material resulting from the smeared shear band approach, and 3) Perform rigorously the nonlinear FE analysis based on the modified initial stress method.

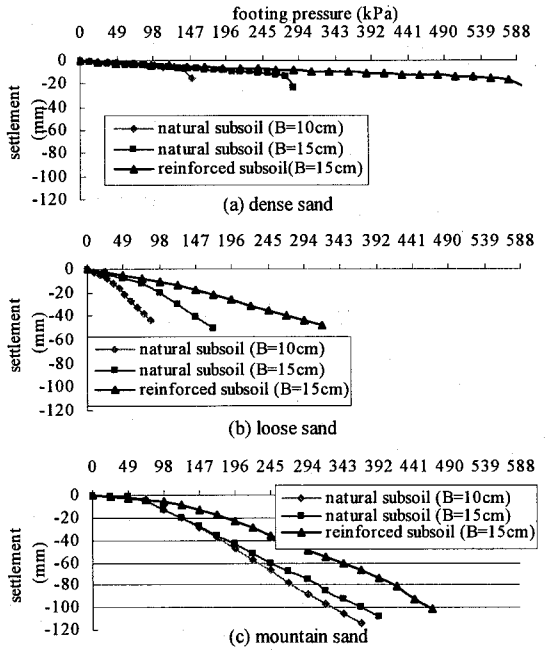

Fig. 6 Effect of earth reinforcement

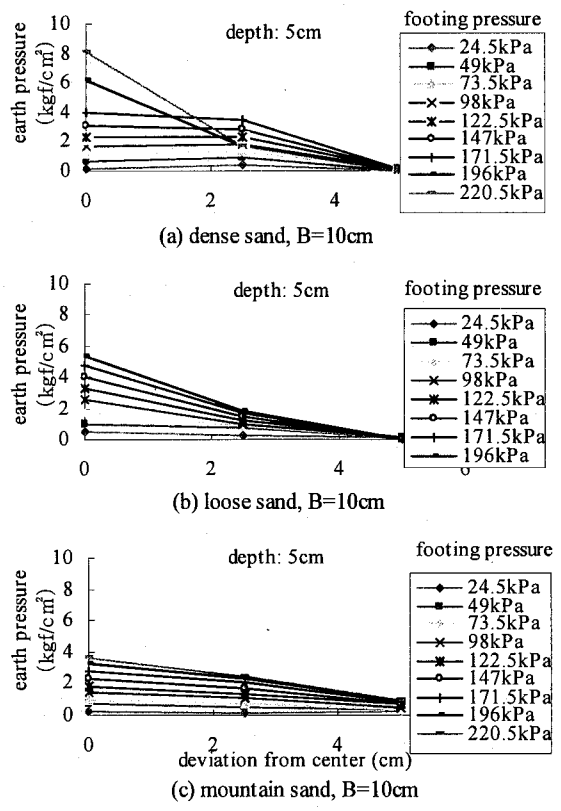

Fig. 7 Distribution of vertical earth pressure

3.2 Yield Criterion

To relate the proposed procedure to conventional stability analysis, Mohr-Coulomb and Coulomb yield criteria are employed respectively to plane strain soil mass and friction interface between structure and soil. For the friction interface we employ the thin layer finite element as shown in Fig. 8[11)].

Mohr-Coulomb:

$$F_M = \{(\sigma_x-\sigma_y)^2+4\tau_{xy}^2\}^{1/2}-\{(\sigma_x+\sigma_y)\sin\phi+2c\cos\phi\} = 0 \quad (1)$$

Coulomb:

$$F_C = |\tau_{st}| - c - \sigma_t \tan\phi \quad (2)$$

where, σ_x, σ_y and τ_{xy}: stress components, and σ_t and τ_{st}: normal and shear stresses in friction interface (see Fig. 8).

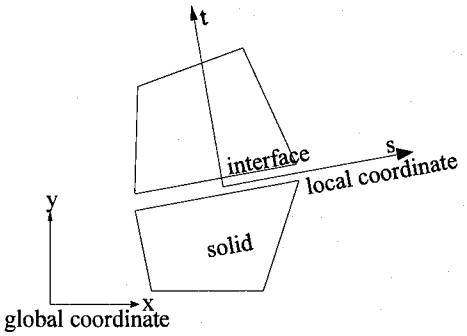

Fig. 8 Coordinates in interface element

3.3 Constitutive Relationship

(1) Stress-strain Relationship for Coulomb Interface

Subjected to Coulomb interface, Fig. 9 schematically illustrates the relationship between stress vector $\{\sigma\}$ and strain vector $\{\varepsilon\}$. Both for Mohr-Coulomb and Coulomb materials, linear elastic responses are assumed before yielding. When

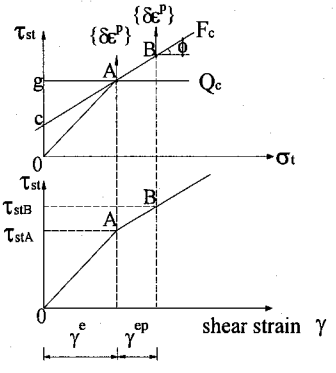

Fig. 9 Stress-strain relationship

applying further footing pressure after yielding, the stress state will move along the yield surface as seen in Fig. 9. This is because normal stress σ_t becomes larger with the increase of footing pressure, and because yielding shear stress increases with normal stress for frictional material. Point B in Fig. 9 corresponds to a plastic equilibrium state at an arbitrary position within a yield region. At the elasto-plastic state from point A to B shown in Fig. 9, we employ a simple non-associated flow rule or plastic potential Q_C defined as [12]

$$Q_C = |\tau_{st}| - g \tag{3}$$

where g: a hypothetical parameter which is not cited actually, because Q_C is used only by its differential form. For the thin layer element shown in Fig. 8, Eqs. (2) and (3) give the elasto-plastic stress-strain relationship as [13]

$$\{\delta\sigma\} = [D_{st}^{ep}]\{\delta\varepsilon^{ep}\} \tag{4}$$

where $\{\delta\sigma\} = \{\delta\sigma_s, \delta\sigma_t, \delta\tau_{st}\}^T$, $\{\delta\varepsilon^{ep}\} = \{\delta\varepsilon_s^{ep}, \delta\varepsilon_t^{ep}, \delta\gamma_{st}^{ep}\}^T$

$$[D_{st}^{ep}] = [D] - [D]\{\partial F_C/\partial\{\sigma\}\}\{\partial Q_C/\partial\{\sigma\}\}^T[D]/\{\partial F_C/\partial\{\sigma\}\}^T$$

$$[D]\times\{\partial Q_C/\partial\{\sigma\}\} = [d_{ij}]$$

$$d_{11}=d_{22}=C_1,\ d_{12}=d_{21}=C_2,\ d_{13}=d_{23}=d_{33}=0,$$

$$d_{31} = \pm C_2\tan\phi\ \ d_{32} = \pm C_1\tan\phi$$

$$C_1 = E(1-\mu)/\{(1+\mu)(1-2\mu)\},\ C_2 = E\mu/\{(1+\mu)(1-2\mu)\}$$

where $\{\delta\sigma\}$ and $\{\delta\varepsilon^{ep}\}$: stress and elasto-plastic strain increments (see Fig. 9), $[D_{st}^{ep}]$: elasto-plastic stress-strain matrix in local coordinate s-t in Fig. 8, [D]: elastic matrix, and d_{ij}: component of $[D_{st}^{ep}]$. The stress and strain components are also defined in coordinate s-t. The upper sign in Fig. 9 corresponds to a positive shear stress.

(2) Stress-strain Relationship for Mohr-Coulomb Material

When shearing a finite size of soil element, it is well known that we often observe a shear band or slip surface as shown in Fig. 10 (a). Despite many theoretical and experimental studies devoted to the mechanism of shear band formation, we still have not reached a final agreement with regard to inclination angle of shear band α defined in Fig. 10 (a) [14)-17)]. Since our main concern is to get a practical design procedure, we employ the most fundamental expression as

$$\alpha = \pi/4 + \phi/2 \tag{5}$$

Without introducing an additional interface element corresponding to a shear band, Pietruszczak et al. [10] proposed the smeared shear band approach which evaluated the average stress-strain response of solid and shear band. Based on this approach, we assume elastic response of solid and elasto-plastic response of shear band herein, because this postulate yields a convenient constitutive behavior as described later. According to the procedure by Pietruszczak et al., the average stress-strain matrix is given as follows. Assume that a plane strain solid element reaches a yield state, and that a shear band has been created as shown in Fig. 10 (a). Regarding the shear band as a thin layer finite element illustrated in Fig. 8, strain components in shear band are given in local coordinate s-t as

$$\{\delta\varepsilon^{ep}\} = [D_{st}^{ep}]^{-1}\{\delta\sigma\} \tag{6}$$

Assuming elastic response except in shear band, strain components in solid region are

$$\{\delta\varepsilon^{e}\} = [D]^{-1}\{\delta\sigma\} \tag{7}$$

Superposing two strains in Eqs. (6) and (7) by smeared shear band approach, average stress-strain matrix of the whole element $[D_{st}^{av}]$ and that in global coordinate x-y $[D_{xy}^{av}]$ is

$$[D_{st}^{av}] = \{[D_{st}^{ep}]^{-1}t/\sqrt{A}\cos\beta$$

$$+[D]^{-1}(1-t/\sqrt{A}\cos\beta)\}^{-1} = [a_{ij}] \tag{8}$$

$$[D_{xy}^{av}] = [T]^T[D_{st}^{av}][T] \tag{9}$$

where t: thickness of shear band, [T]: coordinate transformation matrix, and a_{ij}: component of $[D_{st}^{av}]$. Note that both $[D_{st}^{av}]$ and $[D_{xy}^{av}]$ include no current stress components. Research on shear band thickness demonstrates a_{ij} approaches to d_{ij} defined in Eq. (4) with increasing t. This means that the yield plane strain element becomes close to the stratified or cross-anisotropic material as illustrated in Fig. 10 (b) when t exceeds a certain thickness. In the bearing capacity calculation given later, we can get a collapse mode analogous to Fig. 12 when assuming a_{ij} to be equal to d_{ij}. Considering this result, throughout the following case studies we suppose

$$[D_{st}^{av}] = [D_{st}^{ep}] \tag{10}$$

This assumption means to neglect t. Though the introduction of strain softening may be effective to clarify a collapse point, the proposed procedure considers no softening behavior, because of reducing the number of material parameters for practical use.

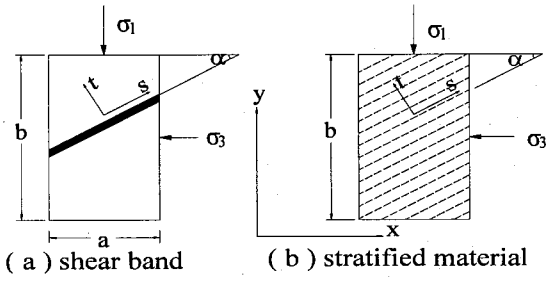

Fig. 10 Shear band formation

(3) Direction of Shear Band

Generally a set of two shear bands or slip surfaces A-A' and B-B' is possible for a finite soil element according to the principal stress state as shown in Fig. 11 (a). In practical problems, it may be troublesome to determine one direction of

shear band, for instance, according to bifurcation analyses. Most of representative stability analyses suppose the active wedge below footing base and often apply the classical passive earth pressure theory in which surface C-C' in Fig. 12 is regarded as a wall surface. Many experimental researches have observed actually the active wedge developed (see Photo. 1). Based on these reasons, we assume the active wedge below footing, which is represented by a series of interface elements in Fig. 8. Considering the above results, we assume the shear band B-B' defined in Fig. 11 (a) within the active wedge in Fig. 12, and assume the shear band A-A' in Fig. 11 (a) outside of the active wedge as seen in Fig. 12. The direction of A-A' or B-B' line in Fig. 11 (b) is generally determined as (see Fig. 11b)

$$\begin{aligned} \beta &= -\alpha - \theta \quad &&: \text{A-A' line} \\ &= \alpha - \theta \quad &&: \text{B-B' line} \end{aligned} \tag{11}$$

where β: inclination angle of shear band from horizontal axis, and θ: angle of the major principal stress from vertical axis. Note that compressive stress is positive here and that shear stress τ_{st} is negative along A-A' line in Fig. 11 (a) and positive along B-B' line.

3.4 Definition of Loading State

As stated above, a stress state is assumed to move along the yield surface after yielding. The linear stress-strain relationship also happens to make a stress state move along left side in Fig. 9 when applying the relationship to a boundary value problem. Such a movement sometimes produces exceedingly high tensile stress for some finite elements[18]. To avoid this confusion, we introduce a constraint with respect to σ_t, which compels a stress state to move along right side in Fig. 9.

$$\delta\sigma_t \geqq 0 \tag{12}$$

Eq. (12) means that normal stress perpendicular to the slip surface never decreases. The finite element, in which stresses violate Eq. (12), is called *tensile element* hereafter.

3.5 Modified Initial Stress Method

With increasing friction angle ϕ, it makes numerical analysis quite troublesome to assume stratified material shown in Fig. 10 (b). The original initial stress method often provides unreasonable distribution of displacement and unstable bearing capacity for the case. In the original stress method, the incremental procedure, which treats the nonlinearity as piecewise linear, does not create the collapse mode as illustrated in Fig. 12, even though assuming the stratified material. This difficulty requires developing a modified initial stress method introduced below. Fig. 13 (a) defines actual stress of initial state $\{\sigma_I\}$, yield stress $\{\sigma_A\}$, actual stress of plastic equilibrium state $\{\sigma_B\}$, elastic stress $\{\sigma_E\}$, virtual initial stress $\{\sigma_0\}$, total strain $\{\varepsilon\}$, elastic strain $\{\varepsilon^e\}$, and elasto-plastic strain $\{\varepsilon^{ep}\}$. For the convenience of solving bearing capacity problems, we apply footing pressure by many loading stages subdivided. In the application of initial stress method, we use the same stiffness matrix throughout all the loading stages, because we assume a linear response of subsoil before yielding and assume a different linear response after yielding as given by Eq. (4). Yield stress $\{\sigma_A\}$ is isolated by Nayak, et al.[19]. To determine the direction of shear band, it is necessary to find direction of the major principal stress θ. We determine θ by using yield stress $\{\sigma_A\}$, and use it throughout the succeeding loading stages, because the other methods do not necessarily provide a collapse mode as shown in Fig. 12.

The original initial stress method is based on an iterative procedure. At each iteration step, the method applies initial stress $\{\sigma_0\} = \{\sigma_E\}-\{\sigma_B\}$ where $\{\sigma_E\}$ is calculated by using $\{\sigma_0\}$ found at the preceding iteration step. Thus the original initial stress method is a special application of the modified Newton-Raphson method from mathematical viewpoint[20]. When applying the original initial stress method together with the constitutive model described above, the numerical results are considerably affected by the finite element subdivision system, and unreasonable distributions of stress and displacement are often observed. These difficulties are avoided by introducing a modified initial stress method, which finds directly the initial stresses without iterative procedure. The constitutive model employed here, which is a linear equation also at the elasto-plastic state, enables to apply the modified initial stress method. Firstly initial stress vector in s-t coordinate is

$$\{\sigma_{st0}\} = \{\sigma_{s0}, \sigma_{t0}, \tau_{st0}\} \tag{13}$$

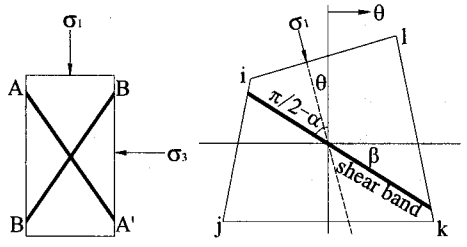

(a) two slip surfaces (b) direction of slip surface in an element

Fig. 11 Direction of shear band

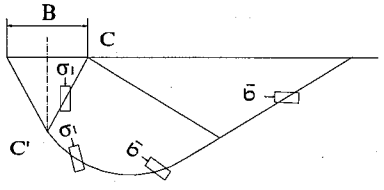

Fig. 12 Isolation of slip surface

Referring to Eq. (4), component d_{ij} in $[D_{st}^{ep}]$ is the same as the component of elastic matrix [D] except the third row components. This means that both σ_{s0} and σ_{t0} in Eq. (13) vanish both in interface and plane strain yield elements. The application of Eq. (13) reduces the numerical effort and clarifies the mechanical meaning of initial stresses. Referring to Fig. 13 (b), in which the stress state has attained to yield state at the present loading stage, the basic equation in the initial stress method is given as

$$\{r\}_i = \{\sigma_{st0}\}_i - [T]_i^{-1}\{\{\sigma_E\}_i - (\{\sigma_A\}_i + \delta\{\sigma_B\}_i)\}$$
$$= \{0, 0, \tau_{st0}\}_i - [T]_i^{-1}([D]_i - [D_{xy}^{av}]_i)([B]_i\{[K]^{-1}(\{\delta f\} + \Sigma_j [B]_j^T [T]_j \{\sigma_{st0}\}_j A_j)\}_i - \delta\{\varepsilon^e\}_i) = 0 \quad (14)$$

where, $\{\sigma_E\} = \{\sigma\}^{n-1} + [D][B]\{\delta u\}$

$$\delta\{\sigma_B\} = [D_{xy}^{av}]\delta\{\varepsilon^p\} = [D_{xy}^{av}][D]^{-1}(\{\sigma_E\} - \{\sigma_A\})$$
$$= [D_{xy}^{av}][D]^{-1}([D][B]\{\delta u\} - (\{\sigma_A\} - \{\sigma\}^{n-1}))$$

where $\{r\}_i$: residual, $[B]_i$: matrix for calculating strain components from nodal displacements, [K]: global stiffness matrix, $\{\delta f\}$: load increment vector, A_j: area of the element, and suffixes i and j denote element number. $\delta\{\varepsilon^e\}$ in Eq. (14) and Fig. 13 is calculated as $[D]^{-1}(\{\sigma_A\} - \{\sigma\}^{n-1})$. The constraint given by Eq. (12) is represented as

$$\{r\}_i = \{\sigma_{st0}\}_i - [T]_i^{-1}\{\{\sigma_B\}_i - \{\sigma_C\}_i\} = \{0, \sigma_{t0}, 0\}_i - [T]_i^{-1}[D]_i([B]_i\{[K]^{-1}(\{\delta f\} + \Sigma_j [B]_j^T [T]_j \{\sigma_{st0}\}_j A_j)\}_i - \delta\{\varepsilon^e\}_i) = 0 \quad (15)$$

where $\{\sigma_C\}_i = \{\sigma_A\}_i$ or $\{\sigma_C\}_i = \{\sigma\}_i^{n-1}$ respectively when the element has yielded at the present loading stage *n* or when the element yielded at the preceding stage. Since both Eqs. (14) and (15) are linear equations with respect to unknown $\{\sigma_{st0}\}$, it is possible to directly solve Eqs. (14) and (15) as a set of simultaneous equations. For instance, Eq. (14) for finite element *i* is given as

$$\{\sigma_{st0}\}_i - [T]_i^{-1}([D]_i - [D_{xy}^{av}]_i)[B]_i\{[K]^{-1}\Sigma_j [B]_j^T [T]_j \{\sigma_{st0}\}_j A_j\}_i = [T]_i^{-1}([D]_i - [D_{xy}^{av}]_i)([B]_i\{[K]^{-1}\{\delta f\}_i - \delta\{\varepsilon^e\}_i) = 0 \quad (16)$$

with respect to unknown $\{\sigma_{st0}\}_j$ given as

$$(\delta_{ij} - |[T]_i^{-1}([D]_i - [D_{xy}^{av}]_i)[B]_i\{[K]^{-1}[B]_j^T [T]_j A_j\}_i|_3)\{0, 0, \tau_{st0}\}_j = |[T]_i^{-1}([D]_i - [D_{xy}^{av}]_i)([B]_i\{[K]^{-1}\{\delta f\}_i - \delta\{\varepsilon^e\}_i)|_3 \quad (17)$$

where $|\ |_3$ denotes the third component of vector, etc. When solving Eqs. (14) and (15), we must assume the constant numbers both of unknown τ_{st0} and σ_{t0}. Thus the following additional iteration is required for determining the yield finite elements and tensile elements. The numerical steps during a typical loading stage are summarized as follows. 1) Performing an elastic analysis by using actual load increment $\{\delta f\}$, calculate $\{\sigma_E\}$ and $\{\delta\varepsilon\}$ in Fig. 13 (b). 2) Find the yield finite elements in which $\{\sigma_E\}$ violate the yield criterion, and tensile elements in which stresses violate Eq. (12). 3) For the yield elements, calculate yield stress $\{\sigma_A\}$ both from $\{\sigma_E\}$ and the preceding stress state. 4) Concerning $\{\sigma_A\}$, calculate direction of the major principal stress θ, and find shear band inclination angle β by Eq. (11). 5) Calculate $[D_{st}^{av}]$ by Eq. (8). 6) Determine $\{\sigma_{st0}\}$ by solving Eqs. (14) and (15). 7) Again, find the yield and tensile elements by performing an elastic analysis by use of both $\{\delta f\}$ and $\{\sigma_{st0}\}$ determined at 6). When finding new yield or tensile elements, determine $\{\sigma_{st0}\}$ subjected to the total yield and tensile elements including the new yield and tensile elements. Repeat this procedure until neither new yield nor tensile element is found. 8) Based on the final results at 7) calculate necessary state variables $\{\sigma_B\}$, settlements, and so on.

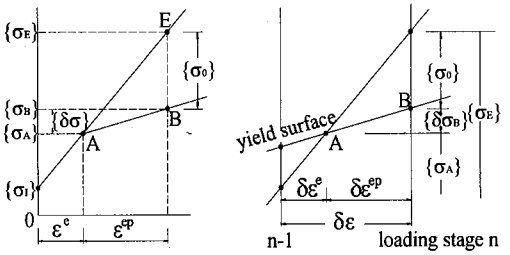

(a) initial stress method (b) initial stress method at a loading stage

Fig. 13 Modified initial stress method

4. Numerical Procedure 2

Numerical procedure 2 is a conventional elasto-plastic FE analysis, in which we employ the stress-strain relationship and non-associated flow rule shown in Fig. 9 without assuming shear band. For Mohr-Coulomb material, the plastic potential is given as:

$$Q_M = \{(\sigma_x - \sigma_y)^2 + 4\tau_{xy}\}^{1/2} - 2g \quad (18)$$

By using Eqs. (1) and (18), the incremental stress-strain relationship is calculated. This problem is successfully solved by the original initial stress method developed by Zienkivicz et al[13].

5. Numerical and Experimental Results

5.1 Hypothetical Case Studies

Fig.15 shows FE meshing for a hypothetical case study. Material parameters are given in Fig. 15, in which γ: unit weight and T: thickness of footing. The footing or loading plate is modeled by beam elements and represented by elastic modulus and moment of inertia. Interface elements are set between footing and soil deposit, in which shear modulus $G = E/2(1+\mu)$. For convenience, we introduce 'footing pressure ratio R' defined as

$$R = q / q_u \quad (19)$$

where q: current footing pressure applied and q_u: ultimate bearing capacity given by Terzaghi[21]. Throughout all the following case studies, angle α in Fig. 15 is given by eq. (5), regarding the vertical footing pressure as the major principal stress. This assumption is valid because the shear stress between footing base and subsoil is quite small before collapse due to small lateral deformation at the upper surface of subsoil. When considering, for instance, coefficient of earth pressure in rest $K_0=1-\sin\phi$[22], the proposed procedures provide much lower bearing capacity than conventional solutions. Thus we give isotropic initial stresses $\{\sigma_I\}$ as follows: σ_{yI}= overburden pressure, horizontal stress $\sigma_{xI}=\sigma_{yI}$, and $\tau_{xy}=0$ as well as assumed in conventional limit equilibrium analyses. Fig. 14 shows R-settlement curves calculated by Numerical procedures 1 and 2. When R exceeds 1.06 in Fig. 14, Numerical procedure 1 gives larger settlement at a loading stage than the settlement at the preceding stage. This suggests that we cannot find a mechanically stable state at the loading stage. Fig. 15 shows the yield region or collapse mode by the procedures for R=1.06. In Fig. 15 (a) a solid line in each finite element represents the direction of shear band defined in Fig. 10, and that the element has yielded. Numerical procedure 1 seems to give a global collapse mode analogous to Prandtl mechanism illustrated in Fig. 12. Note that the collapse mode is represented by stress yield condition as well as the conventional stability analysis. Since Numerical procedure 1 does not sufficiently simulate the strain localization or the concentration of strains, the procedure may not give a complete collapse mode. Fig. 15 (a) suggests that the collapse mode produces an infinite plastic shear flow of subsoil or unreasonable distribution of displacement for R equal to 1.06. Thus we consider R=1.06 as the bearing capacity solution of this problem, which is in good agreement with Terzaghi solution[21]. The bearing capacity in terms of R is called 'critical footing pressure ratio R_{cr}'. The collapse mode in Fig. 15 (a) is supported by the displacement field shown in Fig. 16 (a) and stress filed shown in Fig. 16 (b) that appear mechanically reasonable. The collapse mode is created by considering the weight of subsoil, stiffness of footing and subsoil, friction between footing and subsoil, and stress concentration at the edge of rigid footing in the proposed method, while most of which are ignored in the limit equilibrium approaches. A little difference between the collapse mode in Fig. 15 (a) and Prandtl mechanism is discussed as follows. The yield region in Fig. 15 (a) tends to distribute deeply below footing. Despite the lateral plastic flow as illustrated in Fig. 15 (a), the vertical pressure must reach lower subsoil due to the vertical equilibrium condition, and the pressure makes lower subsoil yield. Although conventional stability analysis provides little information about yield state

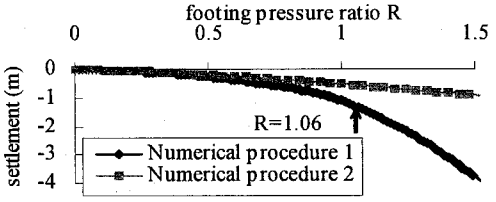

Fig. 14 R-settlement relationship (hypothetical case)

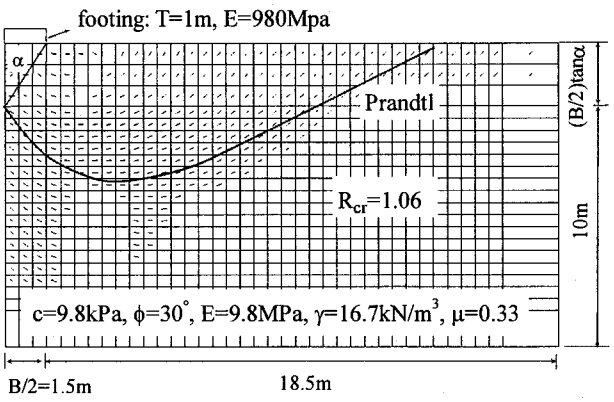

(a) Numerical procedure 1

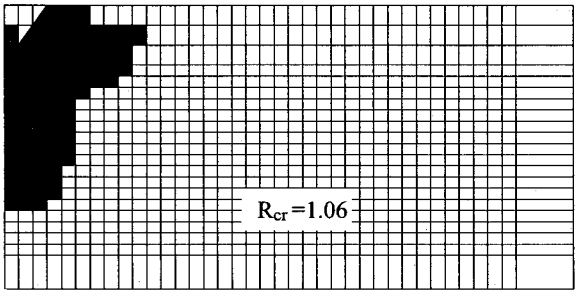

(b) Numerical procedure 2

Fig. 15 Yield region

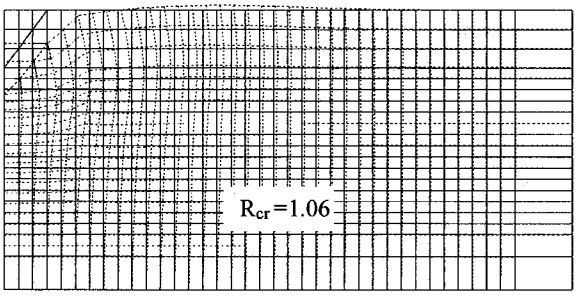

(a) displacement

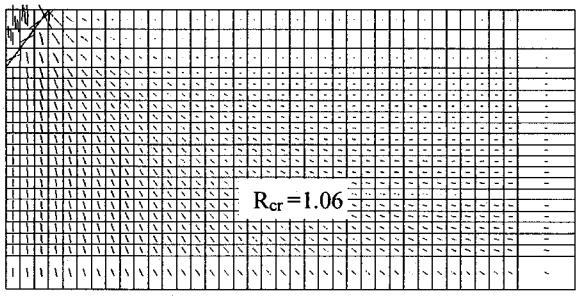

(b) major principle stress

Fig. 16 Displacement and stress field (Numerical procedure 1)

except on the location of slip surface, there is the possibility that the region lower than the slip surface may yield. In Fig. 16 (a) we observe little deformation of lower subsoil. The proposed procedure represents a collapse mode by yield condition of stresses, which is the same as conventional stability analysis and different from most application of conventional FEM using strain distribution. Since Numerical procedure 2 neither constructs a global collapse mode as Numerical procedure 1 nor gives remarkable settlement after exceeding R_{cr}, it is not easy to define R_{cr} explicitly. Numerical procedure 1 gives the settlement larger than Numerical procedure 2, by the plastic shear flow along the sequence of stratified material constructed after yielding.

5.2 Comparison between Numerical and Experimental Results

FE meshing for the experiment is shown in Fig. 17, in which the depth of the active wedge varies with α defined by Eq. (5). Material parameters are given in Table 1. Fig. 18 compares calculated and monitored R-settlement relationships for all the cases listed in Table 1. For Numerical procedure 1, ultimate bearing capacity R_{cr} is given for each case according to the definition stated before. Fig. 19 shows the yield region or collapse mode by Numerical procedure 1 for the above-determined R_{cr}. It contains a slip surface assumed by Prandtl, which is given by assuming no lateral boundary. In any case, Numerical procedure 1 seems to give a collapse mode analogous to Prandtl mechanism. It is not easy to define the bearing capacity by Numerical procedure 2, because the procedure neither constructs a clear collapse mode nor gives a clear turning point in R-settlement curve. Fig. 20 gives examples of yield region by Numerical procedure 2. Fig. 21 shows an example of nodal displacement by Numerical procedure 1.

From Fig. 18, we can observe that Numerical procedure 1 provides larger settlement than Numerical procedure 2 for dense and loose sand due to the reason stated before. Numerical procedure 1 does not intend to simulate stress-strain behavior but to estimate the value of ultimate bearing capacity. Numerical procedure 2 provides somewhat reasonable settlement, but does not give a clear turning point. For mountain sand our procedures cannot consider the characteristic of soft soil with high compressibility, and they provide the calculated results considerably different from monitored ones.

The model test provides R_{cr}=1.0 for B=10cm and R_{cr}=1.36 for B=15cm in dense sand, which are close to Terzaghi solution, while Numerical procedure 1 gives lower bearing capacity. Comparing with Prandtl mechanism in Fig.19, Numerical procedure 1 tends to give more shallow collapse mechanism.

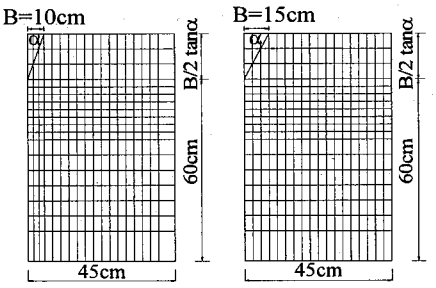

Fig. 17 FE meshing

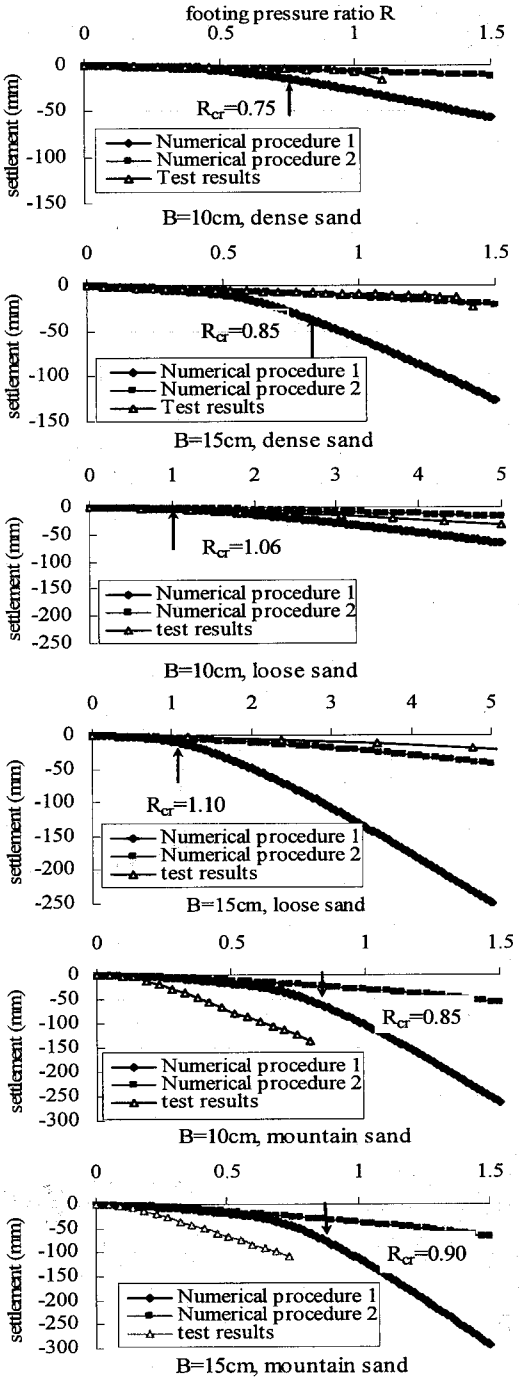

Fig. 18 R-settlement relationship

That is, as shown in Fig. 21, the subsoil deforms upward near the lateral boundary. Numerical procedure 1 may seem to

search the most dangerous collapse mode under the given condition. Note that the procedure gives the similar bearing capacity with Terzaghi solution when foundation soil is sufficiently wide as shown in Fig.15 (a). This tendency may probably reduce the bearing capacity in Fig. 19. One more reason is that Numerical procedure 1 tends to give smaller R_{cr} than Terzaghi solution with increasing ϕ, as shown in Fig. 22.

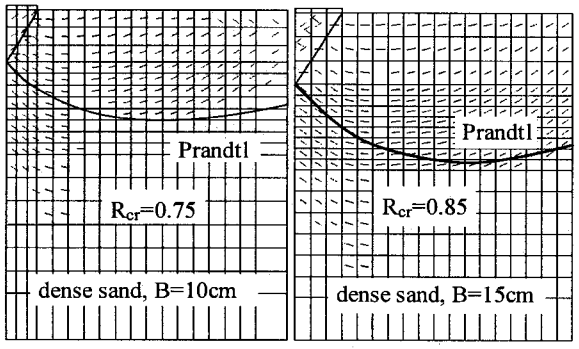

(a) dense sand

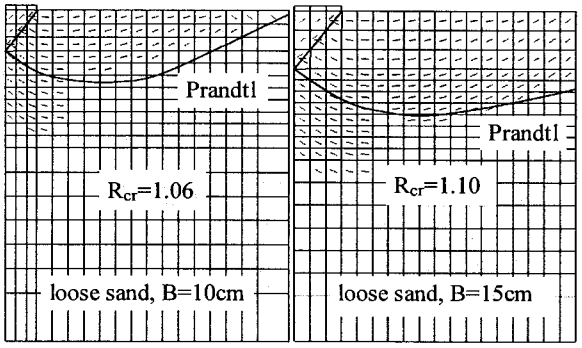

(b) loose sand

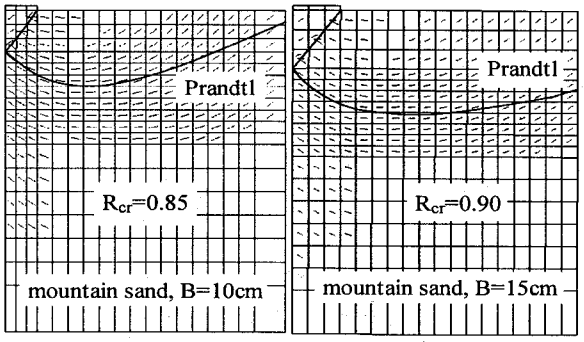

(c) mountain sand

Fig. 19 Yield region (Numerical procedure 1)

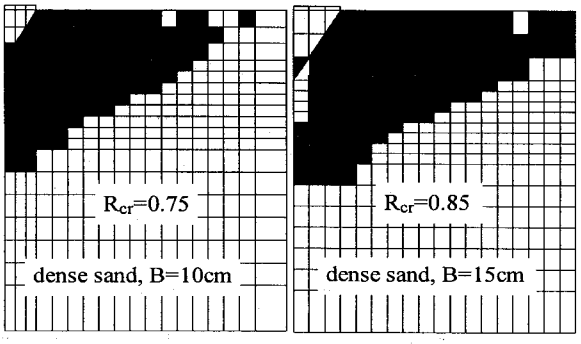

Fig. 20 Yield region (Numerical procedure 2)

For loose sand, Numerical procedure 1 provides R_{cr} close to Terzaghi solution. This is mainly because the collapse mode similar to Prandtl can be formed completely as shown in Fig. 19 (b).

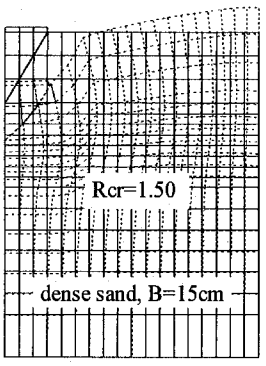

Fig. 21 Nodal displacement (Numerical procedure 1)

Figure 23 compares calculated and monitored distributions of vertical earth pressure. We observe that the large difference between calculated and monitored vertical earth pressures. Experimental results indicate that the earth pressure is large in centerline due to concentration of stress in sands as particulate media. Compared with experimental results, a peak value appears apart from center in Numerical procedure 1. This is because the element at this peak point yields later than others.

Fig. 24 illustrates the earth reinforcement effect on the bearing capacity in comparison with natural subsoil. FE meshing and material parameters are the same as those on

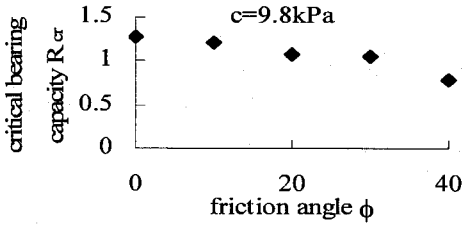

Fig. 22 Effect of ϕ on ultimate bearing capacity

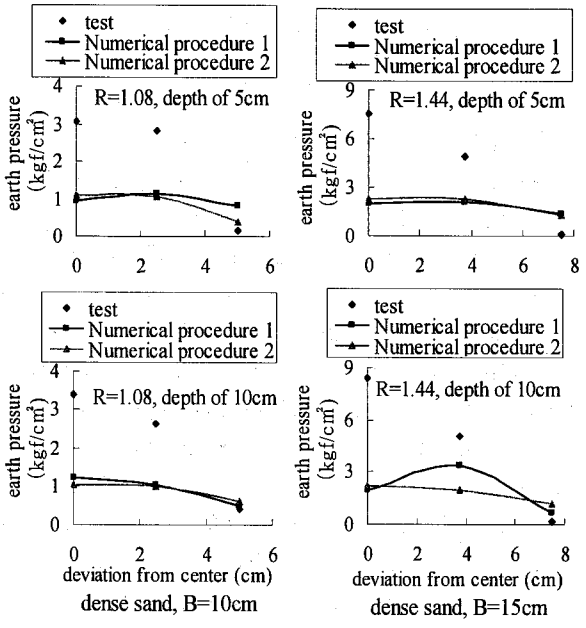

Fig. 23 Distribution of vertical earth pressure

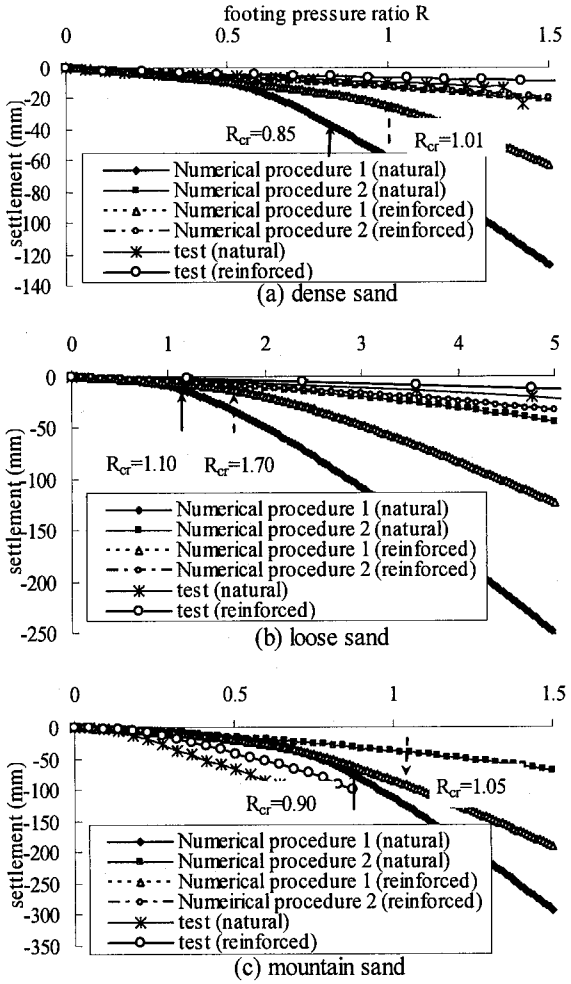

Fig. 24 R-settlement relationship
(comparison between reinforced and natural values)

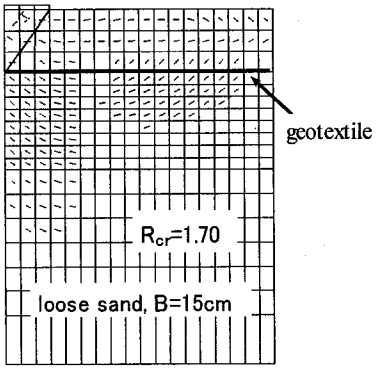

Fig. 25 Yield region (earth reinforcement)

non-reinforced cases except the geotextile is practiced by truss material. The material properties are given in 2.2. In any case the earth reinforcement gives much larger bearing capacity than that in natural subsoil. Since in dense sand the deformation modulus of soil is larger, the effect of reinforcement becomes smaller than the effect in loose sand. Fig. 25 illustrates the yield region for reinforced subsoil in loose sand. As shown in Fig. 24, Numerical procedure 1 restricts the settlement after failure, but the procedure does not give correct solution of settlement after yielding as stated before. Numerical procedure 2 shows a little improvement on bearing capacity and settlement. The conventional ability analysis uses the collapse mechanism assumed without reinforcement, and evaluates the reinforcement material only by its final strength. The method neglects the stiffness of reinforcement material which may restrict the deformation of subsoil and which may largely contribute to the improvement of bearing capacity. This case study proves the possibility of applying the proposed procedure to the stability analysis of earth reinforcement, which takes the stiffness and displacement of material into consideration. The optimal combination of material stiffness with strength, placement etc. will have to be investigated in the future study based on many trial applications of the proposed procedure.

6. Conclusions

This paper performed the laboratory model tests subjected to bearing capacity of rigid strip footing and proposed a numerical procedure for calculating the bearing capacity of strip footing considering stiffness of material and collapse pattern. The procedure aims to fill a gap existing between conventional stability analysis and classical FEM. The procedure employs Mohr-Coulomb and Coulomb yield criteria respectively for soil mass and friction interface between soil and structure. By assuming a linear elastic response before yielding and a simple non-associated flow rule after yielding, and by employing a smeared shear band approach and a modified initial stress method, the procedure provides a collapse mechanism analogous to a slip surface assumed in conventional stability analysis. At the collapse mode created, a stress yield criterion is satisfied as well as along a slip surface supposed in conventional stability analysis. Such a definition of collapse mode is different from most applications of FEM which tend to emphasize plastic shear deformation. Some case studies prove that the proposed procedure provides a solution close to the conventional solution. The procedure produces a collapse mechanism as assumed in conventional stability analysis, and that the mechanism is supported by a displacement field and a stress field. This characteristic indicates the possibility of applying the procedure to the stability analysis which takes stiffness and deformation of material into consideration. Comparisons with experimental results show that the procedure provides a reasonable solution of ultimate bearing capacity but does not give an appropriate settlement after failure. Because this proposed procedure (Procedure 1) does not sufficiently simulate the actual stress-strain behavior. It gives higher value of settlement due to the plastic shear flow along the sequence of stratified material constructed after

yielding. The major purpose of this research is to estimate the bearing capacity by the collapse mode comprised of yielding elements rather than simulate the failure behavior. The procedure should be applied to practical design work to evaluate bearing capacity.

REFERENCES

1) R. de Borst, Vermeer PA.: Possibilities and limitations of finite elements for limit analysis, *Géotechnique,* Vol.34 (2), pp. 199-210, 1984.
2) Frydman S., Burd HJ.: Numerical studies of bearing-capacity factor N_γ, *Journal of Geotechnical and Geoenvironmental Engineering, ASCE*, Vol. 123(1), pp. 20-29, 1997.
3) Lysmer, J.: limit analysis of plane problems in soil mechanics, *Proc. ASCE*, Vol. 96(SM4), pp. 625-640, 1970.
4) Pastor, J., Turgeman, S.: Limit analysis in axisymmetrical problems: numerical determination of complete statical solutions, *Int. J. Mech. Sci.*, Vol. 24(2), pp. 95-117, 1982.
5) Arai, K., Tagyo, K.: Limit analysis of geotechnical problems by applying lower-bound theorem, *Soils and Foundations*, Vol. 25(4), pp. 37-48, 1985.
6) Rundnicki J. W., Rice J. R.: Conditions for the localization of deformation in pressure-sensitive dilatant materials, *Journal of the Mechanics and Physics of Solids*, Vol. 23, pp.371-394, 1975.
7) Ortiz M., Leroy Y., Needleman A.: A finite element method for localized failure analysis, *Computer Methods in Applied Mechanics and Engineering,* Vol. 61, pp. 189-214, 1987.
8) Zienkiewicz O. C., Huang M.: Localization problems in plasticity using finite elements with adaptive remeshing. *International Journal for Numerical and Analytical Methods in Geomechanics*, Vol. 19(2), pp. 127-148, 1995.
9) Hu Y., Randolf M. F.: Deep penetration of shallow foundations on non-homogeneous soil. *Soils and Foundations*, Vol. 38(1), pp. 241-246, 1998.
10) Pietruszczak S., Mroz Z.: Finite element analysis of deformation of strain-softening materials, *International Journal for Numerical Methods in Engineering*, Vol. 17, pp. 327-334,1981.
11) Desai C. S., Zaman M. M, Lightner J. G, Siriwardane H. J.: Thin-layer element for interfaces and joints, *International journal for Numerical and Analytic Methods in Geomechanics*, Vol. 8(1), pp. 19-43, 1984.
12) Mroz Z.: Deformation and flow of granular materials, *Mechanics of Solids (the Rodney Hill 60th Anniversary Volume)*, pp. 119-132, Pergamon Press, Oxford, 1980.
13) Zienkiewicz O. C., Valliappan S., King I. P.: Elastoplastic solutions of engineering problems `initial stress`, finite element approach. *International Journal for Numerical Methods in Engineering*, Vol. 1, pp. 75-100, 1969.
14) Vardoulakis I.: Shear band inclination and shear modulus of sand in biaxial tests, *International Journal for Numerical and Analytical Methods in Geomechanics*, Vol. 4(2), pp. 103-119, 1980.
15) Arther J. R. F., Dunstan T., Al-Ani Q. A. J. L, Assadi A.: Plastic deformation and failure in granular media. *Géotechnique*, Vol. 27(1), pp. 53-74, 1977.
16) Papamichos E., Vardoulakis I.: Shear band formation in sand according to non-coaxial plasticity model, *Géotechnique*, Vol. 45(4), pp. 649-661, 1995.
17) Finno R. J., Harris W. W., Mooney M. A., Viggiani G.: Shear bands in plane strain compression of loose sand. *Géotechnique*, Vol. 47(1), pp. 149-165, 1997.
18) Zinkiewicz O. C., Valliappan S., King I. P.: Stress analysis of rock as a `no tension material`, *Géotechnique*, Vol. 18, pp. 56-66, 1968.
19) Nayak G. C., Zienkiewicz O. C.: Elasto-plastic stress analysis. A generalization for various constitutive relations including strain softening, *International Journal for Numerical Methods in Engineering*, Vol. 5, pp. 113-135, 1972.
20) Stolle D. F. E.: An interpretation of initial stress and strain methods, and numerical stability, *International Journal for Numerical and Analytical Methods in Geomechanics*, Vol. 15(6), pp. 9-416, 1991.
21) Terzaghi, K.: *Theoretical Soil Mechanics*, New York, 1943.
22) Jáky J.: Pressure in soils, *Proc. of 2nd ICSMFE*, Vol. 1, pp. 103-109, 1948.

(Received April 12, 2007)